Gas Embolism on a Chip: Mimicking Iatrogenicity at the Microscale

K. Baassiri**, L. Maskova**, M.M. Mardanpour**, T. Allen, F. Gamper, A.F. Asomoza, A.S. Perumal, and D.V. Nicolau*, *Member, IEEE*

***Abstract* — *Objective*: Gas embolism (GE) is a potentially life-threatening condition with difficult *in vivo* investigation. The physical nature of the initial stages of GE makes *in vitro* abiotic microfluidics valuable for phenomenological studies. A versatile microfluidic system was used to mimic the microscale iatrogenic GE during gastroscopy, laparoscopy, and hyperbaric therapy under three scenarios: gas transfer through perforated or non-perforated microvasculature, and via tissue supersaturation. *Methods*: Polydimethylsiloxane devices mimicking microvascular geometries, with, or without injuries, hosted the flow of artificial blood. Localized gas pressures comparable to those used in gastroscopy, laparoscopy, and hyperbaric therapy were applied on microvasculature using air, carbon dioxide or /nitrogen to mimic microscale GE. *Results*: Air and carbon dioxide produced markedly different GE patterns. Air generated numerous small bubbles across the entire pressure range, and a distinct population of larger emboli at lower pressures. Conversely, carbon dioxide embolism occurred beyond a threshold pressure (23-58 mm Hg), but once initiated, complete blockage or continuous gas injection lasting tens of seconds occurred. *Conclusion*: Air embolism may occur in injured microvasculature at pressures within the lower range encountered during gastroscopy. Carbon dioxide embolism requires higher pressures, but once triggered, it can result in high-volume gas entry during laparoscopy. High pressure gas-supersaturated tissues can act as gas 'reservoirs' prolonging GE therapy. *Significance*: These findings underscore the risk of air GE in gastroscopy and the need for pressure *and* flowrate control; possible carbon dioxide GE during laparoscopy warrants further assessment; and the duration of gas clearance during GE therapy needs to be considered.**

***Index Terms*—Gas embolism, laparoscopy, gastroscopy, microfluidics**

I. Introduction

VASCULAR gas embolism is a medical condition characterized by the presence of gas bubbles (or in the medical context, gas emboli), in the circulatory system, where they can lodge and obstruct blood flow[1]. The evolution of gas embolism involves two parallel, but temporally distinct pathways[2]. The first, fast physical path encompasses rapid formation of gas emboli and the development of a protective membrane around the bubbles, that delays their dissolution into the bloodstream. This process can result in mechanically obstructed blood vessels, reducing red blood cell (RBC) perfusion and impairing oxygen delivery to tissues and organs[2]. A second, slower biochemical and biological path involves a cascade of cellular and molecular responses, including the formation of white and red thrombi, inflammation, oxidative stress, cellular injury, tissue hypoxia, and organ dysfunction[3-5].

Gas embolism may arise through several mechanisms. Systemic gas embolism occurs when pressure changes affect the entire body, i.e., in diving[2], and high altitude activities[6]. Meso-scale gas embolism results from pressure variations localized to specific anatomical regions [7,8], such as those associated with blunt thoracic trauma[9,10], forceful cardiopulmonary resuscitation[11], pulmonary over-expansion injury[12], explosions[13], and even childbirth[14]. Finally, local gas embolism results from accidental or intentional introduction of gas into the vascular system, or from the *in situ* generation of bubbles within blood vessels[15].

While gas embolism is *reported* as a rare medical condition, particularly in iatrogenic circumstances[16], the symptomatic cases of gas embolism pose significant danger, with mortality rates[17] from 8-12%[18] to 46%[19], or severe neurological sequelae[20,21] in 9 to 35% of survivors[18]. These outcomes are partly caused by late diagnosis, which frequently occurs only after neurological symptoms become apparent. By this stage, however, critical organs may have sustained significant injury, as tissue damage can develop within minutes, particularly in the brain[22].

Several factors complicate the rapid diagnosis and treatment of gas embolism. Initially, gas embolism is purely a physical phenomenon, with biochemical and cellular responses emerging later. Consequently, conventional laboratory tests offer little diagnostic value within the narrow therapeutic window required for effective intervention[23]. In principle, medical imaging, i.e., ultrasound and magnetic resonance imaging, can visualize gas emboli. However, their utility for early diagnosis is limited by the uncertain location of emboli in the body, the need for immediate access to imaging equipment, and the rapid progression of this medical condition[24]. These constraints hinder timely intervention before administration of the only established treatment, hyperbaric oxygen therapy.

Submitted for review on 2 May 2025. This research was funded by the Canadian Natural Sciences and Engineering Research Council (NSERC), grant no. RGPIN- 2022-04053.

K. Baassiri, L. Maskova, M.M. Mardanpour, T. Allen, F. Gamper, A.F. Asomoza, A.S. Perumal and *D.V. Nicolau are in the Department of Bioengineering, Faculty of Engineering, McGill University, Montreal, Quebec, H3A 0E9, Canada. ** Authors who contributed equally. Correspondence e-mail: dan.nicolau@mcgill.ca.

These challenges, both fundamental and practical, contributed to a relative decline in research activity on gas embolism, as reflected by a marked reduction in the number of published reports compared with previous decades[25]. This decline is particularly concerning because virtually all medical and surgical specialties can potentially induce local gas embolism. Documented causes include laparoscopy, gastroscopy, angiography, hemodialysis, coronary artery bypass surgery, central venous catheterization[26], lung biopsy[27], and wound irrigation[15, 28]. The limited attention to this condition is further reflected in the wide variability of reported incidence rates[29], ranging from 0.005% for arterial[30], to 10-50% for venous gas embolism[31]. In laparoscopic surgery alone, the reported incidences reach 50% in pediatric appendectomy[23], 70% in cholecystectomy[32], and 100% in total hysterectomy[33].

Given the broad spectrum of clinical contexts affected, gas embolism is rapidly emerging as a critical complication in emergency units[12-14]. In particular, the rising prevalence of invasive medical procedures involving pressurized gases, e.g., laparoscopy, gastroscopy, automated radiological, bubble-containing injections for ultrasound imaging, will inevitably lead to a surge in iatrogenic cases of gas embolism. The risk increases in patients with compromised vascular integrity, including elderly and obese individuals, as well as patients with cardiovascular or pulmonary disorders such as atherosclerosis, vascular malformations, or previous surgical interventions[34].

Because most iatrogenic gas emboli originate locally, reproducing these phenomena at microscale is particularly relevant. Furthermore, the difficulty of visualizing gas emboli *in vivo* highlights the value of controlled *in vitro* investigations. Finally, the physical nature of gas embolism during its earliest stages also underscores the use of abiotic systems that mimic the microvascular environment. Fortunately, microfluidic platforms are well suited for this purpose, offering precise control of microscale flow conditions and enabling real-time observation of relevant phenomena[35, 36]. Indeed, microfluidic technologies are progressively used to model diseases and medical conditions, e.g., organs-on-a-chip[23, 37-40]. Notable examples include airway-on-a-chip[41] and alveolus-on-a-chip platforms[42, 43], as well as a recently developed advanced 3D construct[44] providing high-precision biomimetic alveolar structures.

Several studies employed microfluidic approaches to investigate the evolution, dissolution, and biological effects of artificially generated gas bubbles. A series of experimental and computational studies[45-47] focused on the impact of bubble formation on blood flow at cellular level, i.e., the cell-free layers and concentrations of RBCs within bifurcating microvascular networks. Another study[48] explored the effect of direct mechanical interaction between gas bubbles and cells. Most recently, the influence of air-to-liquid ratios on flow behavior in Y-shaped and T-shaped microchannel junctions was analyzed across a range of vessel diameters and hematocrit-equivalent concentrations[49]. However, these studies relied on externally injected gas, therefore omitting the actual origins of bubble formation.

The present work investigated bubble formation resulting from the use of pressurized gases in medical procedures. This mechanism is likely one of the principal causes of iatrogenic gas embolism, notwithstanding direct introduction of gas into blood circulation, e.g., intentional for ultrasound imaging, and accidental, e.g. wrong catheterization. In particular, the study reproduces conditions relevant to gas insufflation in gastroscopy (using air) and laparoscopy (using carbon dioxide).

II. MATERIALS AND METHODS

A. Microfluidic Design and Experimental Setup

Polydimethylsiloxane (PDMS) microfluidic devices comprised an artificial vascular channel (30 to 250 µm width) separated from a square pressure cavity (1 mm^2) by a PDMS wall of controlled thickness (25, 50, and 75 µm). To mimic a vascular injury, a second series of devices incorporated a perforation (with calibrated widths of 16, 32 or 100 µm) connecting the pressure cavity to the vascular channel. The overall experimental system and device design are detailed in Fig. 1, while fabrication details are provided in Supplementary Information (SI.1).

The experimental setup consisted of an inverted confocal microscope (Olympus IX83 fluorescence microscope, Olympus Corporation), gas and working fluid delivery systems, and PDMS microfluidic device (Fig. 1). Working fluids pumped through the artificial blood vessels included distilled water and artificial blood analogue. Distilled water served for preliminary system validation, while the blood analogue was employed for all detailed investigations. The blood analogue reproduced the physical properties of human blood with 46% hematocrit concentration (3.5 to 5.5 cP viscosity [48] and surface tension 53 to 58 mN/m [49]). The artificial blood solution consisted of 60% distilled water and 40% glycerol by volume, with xanthan gum added at 0.04 wt.% to achieve the desired shear viscosity[50]. Although PDMS channels enabled direct visualization of gas-liquid interfaces, a fluorescent tracer aided imaging and analysis when enhanced contrast was required. Fluorescein sodium salt (Fischer Scientific) was added to the working fluid at a concentration of 2 mL of a 2 wt.% stock solution per 100 mL of working fluid.

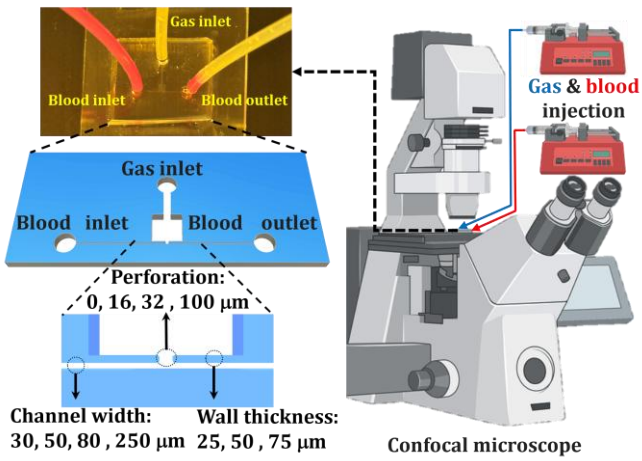

Fig. 1. Experimental setup with zoom in on the setup of the microfluidic device and vasculature geometry

Detailed description of the fluid delivery systems and device storage is provided in SI.2 and SI.3, respectively. The calculations of applied pressures for each case and the statistical data for experiments are detailed in SI.4, Table SI.1-2, and Fig. SI.3.

B. Image Processing

All still images and videos were acquired at sub-millimeter resolution, and the imaging windows for dynamic runs were determined by a fixed number of frames per trial. Videos for air and nitrogen experiments featured a framerate of 50 fps with a 20 ms exposure time, producing recordings of up to 142s. This acquisition rate provided sufficient temporal resolution to capture rapid bubble formation and rupture dynamics. In contrast, carbon dioxide exhibited substantially slower dynamics due to the higher solubility of carbon dioxide and longer timescale required for bubble nucleation and growth. Consequently, a 1 fps framerate with a 10 ms exposure time enabled extended observation periods while minimizing data volume. Subsequent data analysis was conducted using ImageJ, a Java-based image processing program[53], and a custom-developed MATLAB script (SI.5).

III. RESULTS AND DISCUSSION

A. Physical Processes During Medical Procedures Using Insufflation

In laparoscopy, the insufflation gas is almost fully confined in a closed volume, i.e., the pneumoperitoneum, thus exerting continuous pressure on peritoneum and exposed organs throughout the procedure. Carbon dioxide is widely used in laparoscopy because its high solubility in blood reduces both the likelihood and persistence of gas emboli compared with low-solubility gases such as nitrogen or air. In blood, carbon dioxide is transported in multiple forms. A large fraction is converted to bicarbonate, another smaller fraction binds to hemoglobin within red blood cells as carbamino compounds, and only a minor fraction remains physically dissolved in plasma. This multi-pathway transport, involving both plasma and red blood cells, provides blood with a substantially greater effective uptake capacity for carbon dioxide than for nitrogen, which relies solely on physical dissolution[54]. Consequently, carbon dioxide bubbles dissolve more rapidly and exhibit shorter persistence than nitrogen or air bubbles. However, despite this high uptake capacity, the absorption of carbon dioxide by blood is still expected to be considerably slower than the initial formation of gas emboli. A more detailed discussion of carbon dioxide transport is provided in Section SI.6.

At the start of a laparoscopic procedure, carbon dioxide is introduced into the peritoneal cavity through a Veress needle at flow rates of 4000-6000 mL/min to establish intra-abdominal pressures of 10-20 mm Hg above atmospheric pressure[55-57]. The operative space is maintained by a continuous gas supply of 200 to 400 mL/min throughout the entire surgical procedure, typically lasting from 30 to 60 min[56]. Notably, these operating pressures correspond to only 1-2% increase above atmospheric pressure (in absolute units). Such a narrow pressure margin can be susceptible to fluctuations, particularly during the initial insufflation phase or following gas leakage caused by instrument manipulation, potentially leading to relative pressures higher than those in the blood vessels. Furthermore, residual postoperative gases only dissipate within 3 days in approximately 81% of patients and within 7 days in 96% of patients[58]. Withing this timeframe, the gas continues to exert pressure on internal tissues.

Medical use of gastroscopy includes diagnosis of upper gastrointestinal disorders, including ulcers, inflammation, and tumors, as well as minimally invasive therapeutic interventions such as tissue biopsy and endoscopic ligation of bleeding esophageal vessels[59]. Like laparoscopy, the procedure relies on gas insufflation, most commonly using air, to create an adequate working volume. However, in contrast to laparoscopy, the insufflated air is not fully contained and can be partially released through eructation, thus reducing the degree of pressure confinement. Gastroscopy is generally less standardized than laparoscopy and relies more heavily on operator's experience[60]. In addition, insufflation pressure is commonly regulated indirectly through manual adjustment of the air flow rate rather than direct pressure control. A typical gastroscopy procedure lasts approximately 10 mins, during which insufflation flow rate may reach 1.8 L/min[61], i.e., approximately six times higher than the maintenance flow rate in laparoscopy. Despite being rather common, and even performed at outpatient clinics, gastroscopy can lead to side effects ranging from abdominal pain or bloating to spontaneous rupture of the esophagus or gas embolism[62]. Because of the lack of standardization or 'personalization', the achieved gas pressures are rarely reported, and they are rather varied. For instance, a recent *in vivo* study reported esophageal and gastric relative pressures of 9 and 10 mm Hg, respectively, with transient spikes reaching up to 60 mm Hg (depending on the operating surgeon)[60]. In contrast, an *in vitro* investigation reported relative gas pressures ranging from 180 to 300 mm Hg, depending on the endoscope circuit setup[61]. While colonoscopy and sigmoidoscopy share similar framework, the procedures are even less standardized regarding applied pressures, and gas embolism appears to be more rare.

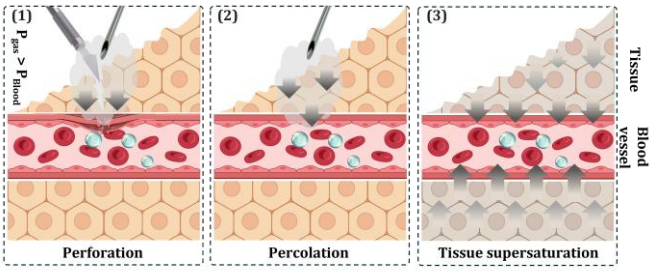

Fig. 2. Schematic representation of iatrogenic gas embolism in laparoscopy or gastroscopy, occurring following Scenario 1: accidental, inevitable, or preexisting damage to blood vessels; Scenario 2: gas percolation; and Scenario 3: ex-diffusion from tissue supersaturated with gas. The arrowheads represent gas flow direction.

In principle, there are several mechanisms for the entry of pressured gas into the circulatory system, schematically presented in Fig. 2, in relatively decreasing order of likelihood:

A.1. Scenario 1. Direct injection of gas through microvascular injuries. Direct gas entry through perforated blood vessels is likely the most important mechanism underlying iatrogenic gas embolism, given the high probability

of vascular injury during tissue manipulation in laparoscopy or gastroscopy. Once a perforated blood vessel gets into contact with the surrounding pressurized environment, two distinct situations may arise, depending on the balance of pressure between gas and blood. If the intravascular pressure exceeds the external gas pressure, blood exits the vessel and bleeding becomes apparent, typically prompting corrective measures such as cauterization. Conversely, if the blood pressure is lower than the applied gas pressure, overt bleeding will not occur. Under these conditions, a pressure gradient is established that favors gas entry into the circulation, potentially allowing gas emboli to form without immediate clinical detection. While the physical principles of gas injection due to negative pressure gradient are similar, there are some specificities related to laparoscopy and gastroscopy.

(i). During laparoscopy-assisted surgery, the initially exposed surfaces of abdominal organs contain relatively large blood vessels with thicker walls and higher intravascular pressures, making them less susceptible to gas intrusion. However, the operative phase often requires incision and manipulation of internal tissues, exposing progressively smaller vessels characterized by thinner walls and lower blood pressures. These vessels are more prone to perforation or complete transection and, thereby, gas intrusion. Clinical observations support this mechanism. For example, a recent study of laparoscopic appendectomy reported that all cases of gas embolism occurred during the operative phase of the procedure, accounting for approximately half of all patients studied[23]. In addition, vascular injury to the surface-facing blood vessels may result from routine instrument manipulation[38, 63], including insertion of the Veress needle, which benefits from minimal visual guidance[64]. Importantly, blood pressures within the smaller blood vessels are substantially lower than the insufflation pressures commonly employed during laparoscopy. Pressures in small venules may be approximately 10 mm Hg[65], and can go as low as 3 mm Hg in the smallest vessels[66]. These blood pressures are considerably below the surrounding relative gas pressure used in laparoscopy, i.e., 10-20 mm Hg. Consequently, a pressure gradient favorable to gas entry may readily develop whenever vessel integrity is compromised. Furthermore, if gas escapes from the pneumoperitoneum into injured vessels, the insufflation system may interpret the resulting pressure drop as leakage and compensate by increasing gas delivery, potentially reinforcing the driving force for continued gas entry.

(ii). Gastroscopy is primarily a diagnostic procedure, although therapeutic interventions such as biopsy or ligation may also occur. Under normal conditions, the blood vessels exposed along the esophageal and gastric mucosa possess relatively robust walls and higher intravascular pressures than those found within the exposed organs. However, the gastrointestinal lining frequently contains pathological vessels, including sclerotic, fragile, or actively bleeding ones, which are prone to further damage during the procedure. The risk of gas entry via the injured vessels is amplified by the potentially high insufflation pressures achieved during gastroscopy. Recent *in vivo* measurements reported transient pressure peaks of up to 60 mm Hg[60], exceeding the pressures found in venules and many small veins. Even higher values, ranging from 180 to 300 mm Hg depending on endoscope configuration, were reported under *in vitro* conditions[61]. These pressures exceed those present in blood vessels substantially larger than arterioles (Fig. 3), creating a strong driving force for gas injection through vascular defects. Finally, the use of air further increases the risk of clinically significant gas embolism. Compared with carbon dioxide, air exhibits 20-25 times lower

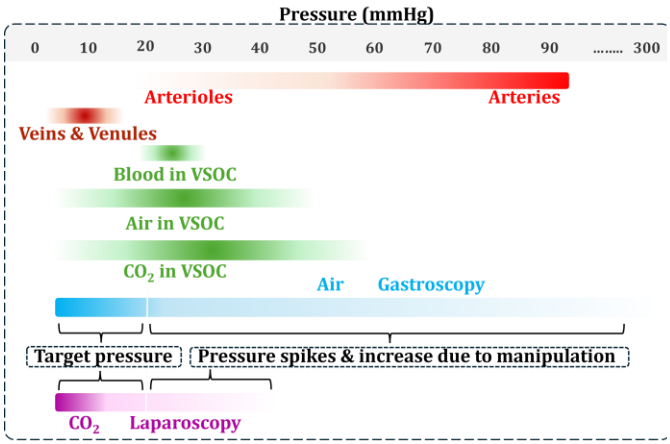

Fig. 3. Schematic representation of pressure ranges relevant to this study: blood pressure in arterioles, venules, VSOC, gas pressure studied in VSOC, and reported air and carbon dioxide pressures in gastroscopy and laparoscopy, including reported spikes and increases due to instrument manipulation.

solubility in blood[67], leading to slower dissolution of emboli. Consequently, even small volumes of entrapped air may pose a greater risk than comparable volumes of carbon dioxide.

A.2. Scenario 2. Percolation of gas through physically intact walls of blood vessels. In principle, gas emboli may form even in the absence of overt vascular injury. When blood vessels are exposed to sufficiently high external gas pressures, gas transport across the vessel wall may exceed the rate at which the dissolved gas can be removed by the bloodstream. Under such conditions, gas may penetrate the vessel wall and enter the circulation in the gaseous phase through percolation. The likelihood of this mechanism increases for thinner vascular barriers and higher external gas pressures. Importantly, this scenario happens below the threshold of mechanical failure of the vessel wall. Once rupture occurs, direct gas entry through vascular defects (Scenario 1) dominates.

A.3. Scenario 3. Ex-diffusion of gas from the supersaturated surrounding tissues. A third potential mechanism involves the delayed release of gas from tissues supersaturated by prolonged exposure. Because gas clearance from tissues is generally slower than that from circulating blood, a transient state may arise in which the bloodstream has already returned to equilibrium while the surrounding tissues remain supersaturated. The resulting concentration gradient can then drive gas diffusion from the tissues into the bloodstream, potentially leading to bubble nucleation long after the initial emboli were removed from blood. This situation becomes relevant during prolonged exposures, e.g., extended diving activities, or during hyperbaric oxygen therapy (HBOT).

B. Mimicking Embolism Conditions in Medical Environments Using Pressurized Gas

Investigating the early, physics-dominated stages of iatrogenic gas embolism required an *in vitro* platform capable of reproducing key features of the microvascular environment exposed to insufflation gases. The designed vascular-system-

on-a-chip (VSOC) emulated relevant physiological characteristics such as tissue mechanical properties, blood rheology, vascular dimensions, and pressure conditions.

B.1. Materials. The material selected to mimic the vascular environment must reproduce the mechanical and transport properties of biological tissues, particularly their elastic response (Young's modulus) and gas diffusivity. PDMS was the preferred candidate because its properties fall within ranges relevant to soft biological tissues[68, 69] (Table 1). Furthermore, these properties can be adjusted by pre-polymer composition, curing protocols, presence of additives[70], and plasma treatment[71], enabling controlled approximation of specific physiological conditions. Finally, PDMS is optically transparent, facilitating direct visualization of gas-liquid interface, and remains one of the most widely used materials in microfluidics owing to its well-established and reproducible manufacturing protocols[52].

TABLE I
MICROVASCULATURE MIMICRY USING PDMS MICROFLUIDICS

Vasculature → Parameter↓	Arterioles	Venules	VSOC
Channel width (μm)[2,93]	10-300	10-100	30-250
Wall thickness (μm)[94]	20	2	25-75
Flow rate (μL/h)[95]	3.61-1060	3.63-159	20-770
Young's modulus (MPa)[96,97]	0.05-1.00	0.01-0.20	0.05-5
Diffusivity (·10^{-5} cm^2/s) [98-103]	1-2.35	1-2.35	1.4-3.7
Blood pressure (mmHg)[104,105]	30-40	10-15	19-31
Re	≤1	≤1	0.04-0.4
Wall shear stress	1.0-7.0	1.0-7.0	3.0-15.0

B.2. Fluids. Precisely formulated artificial blood can closely replicate the rheological properties of human blood within the normal range of hematocrit concentrations[72]. Hereby, the flow dynamics within the microchannels is expected to accurately simulate blood flowing through vessels, as indicated by the Reynolds number and wall shear stress (Table 1).

B.3. Geometry of Microvasculature. The dimensions of artificial blood vessels represented the size range of small blood vessels (Table 1). The liquid pressures measured in our setup varied slightly with channel size/liquid flow rate, yielding values of 19 ± 7 mm Hg (30-80 μm channels) and 31 ± 9 mm Hg (250 μm channel). These pressures fall within the range reported for arterioles and venules (below 40 mm Hg)[73], indicating that the system reproduced physiologically relevant pressure conditions. To investigate gas entry through damaged vessels (Scenario 1), selected devices incorporated a 50 μm-long wall perforation connecting the pressure cavity and the vascular channel. Perforation widths of 16, 32, and 100 μm represented varying degrees of vascular injury. The adjacent 1 mm^2 square-shaped pressure cavity enabled controlled application of external gas pressure, reproducing the localized pressure gradients encountered during insufflation procedures. In this configuration, the device allowed direct investigation of gas entry through vascular defects. The same platform, using channels without perforations, was employed to investigate gas transport across intact vessel walls (Scenario 2). This geometry mimicked the role of the tip of the Veress needle during laparoscopic procedures, and the localized pressure applied at the end of the endoscope in gastroscopy. The same system was used for Scenario 3, i.e., ex-diffusion from oversaturated artificial tissue.

B.4. Operation of microfluidic system. Experimental conditions closely reproduced the physiological and procedural environments associated with laparoscopy and gastroscopy. Flow rates of artificial blood matched those reported for blood vessels of comparable dimensions (Table 1). The applied gas pressures encompassed the operating ranges of the corresponding medical procedures, including transient pressure elevations that may arise during insufflation, gas leakage, or surgical instrument manipulation[74] (Fig. 3). Where necessary, the pressure range was extended beyond typical clinical values to facilitate observation of bubble formation.

C. Scenario 1: Bubble Generation in Microvasculature with Calibrated Perforations

Incorporating calibrated perforations in the vascular channel aimed to mimic direct gas entry into circulation through damaged blood vessels, as may occur as a consequence of surgical incision or pre-existing vascular pathology (Fig. 2). In this instance, gas embolism occurred when the external gas pressure exceeded the pressure of the flowing liquid enough to allow gas to penetrate the artificial vessel through the perforation. Because the liquid pressure varied only slightly among the tested configurations, applied gas pressure and system geometry had the main influence on bubble formation and subsequent flow behavior.

C1. Mimicking air embolism. For air gas embolism (pressure 4.54-42.74 mm Hg) in blood vessels with a wall thickness of 50 μm (nominal value for all subsequent experiments) the observed phenomena included:

(i) Small perforations (16 and 32 μm) *and* small blood vessels (30 and 50 μm) (A1, A2, B1, and B2 in Fig. 4) presented a sizable minority of larger gas bubbles at low pressure.

(ii). Conversely, vessels with larger perforations, i.e., 100 μm (column C in Fig. 4), displayed a more uniform distribution of bubble volumes across the investigated pressure range.

(iii). Large air bubbles formed, sporadically, below 15 mm Hg (Fig. 4; especially in A4 - 250 μm channel/16 μm perforation, and in C2 - 50 μm channel/100 μm perforation). The genesis of large bubbles at low pressures can be explained by the buildup of pressure within the system, resulting in chaotic bubble formation and broad distribution of bubble sizes.

To evaluate the physiological significance of generated emboli, further analysis focused on translating bubble volume into corresponding length of Taylor bubbles in blood vessels of various widths. Taylor bubbles are elongated, sausage-shaped gas structures that occupy most of the cross-section of a confined channel and therefore provide a useful approximation of emboli dimensions in microvessels. The geometry of human (and mammalian) microvasculature system follows Murray's law[75, 76], which relates the diameters of parent and daughter vessels. A comprehensive review [77] reported that the average ratio of the distance separating two bifurcations and the diameter of the respective blood vessel is approximately 10.37.

The lengths allowed the comparison with the characteristic distance between consecutive vascular bifurcations (Fig. 5).

(i). In small vessels numerous emboli reached or exceeded the characteristic inter-bifurcation distance (50 μm and more prominently 30 μm), especially for small perforations.

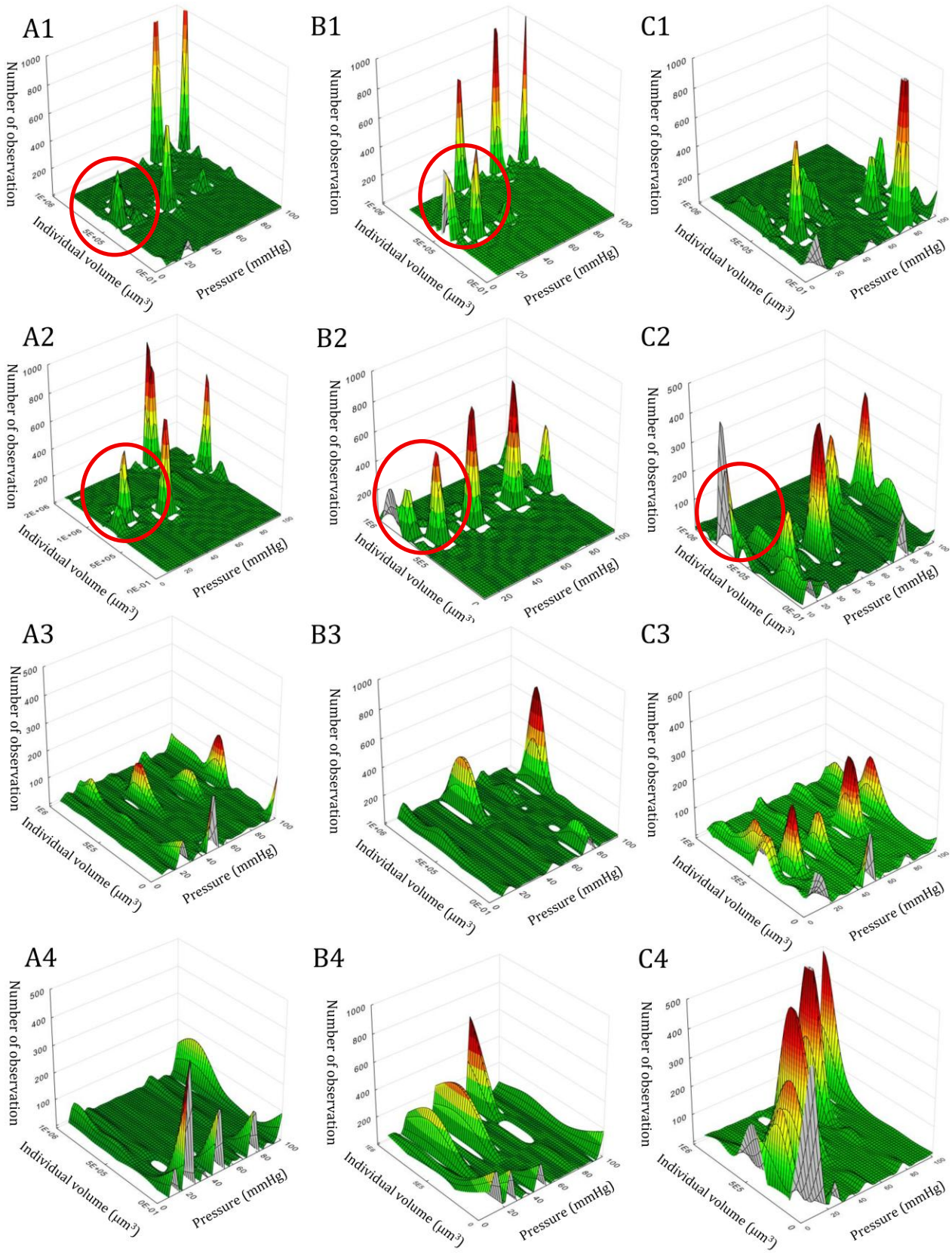

Fig. 4 Distribution of the volumes of air bubbles versus applied air pressures (similar to those used in gastroscopy) on channels with perforated walls, for perforations with 16 μm widths (A column), 32 μm widths (B column), and 100 μm widths (C column), into artificial blood vessels with widths of 30 μm (first row), 50 μm (second row), 80 μm (third row), and 250 μm (forth row). Note the sizable minority of large bubbles (red circles) for small perforations *and* small blood vessels (A1, A2, B1, B2, and C2). Conversely, for large perforations and large blood vessels the distribution of the sizes of bubbles follows an expected progression of larger sizes for larger pressures, reaching a near linear relationship for the largest perforation (100 μm) and largest blood vessel (250 μm) in C4.

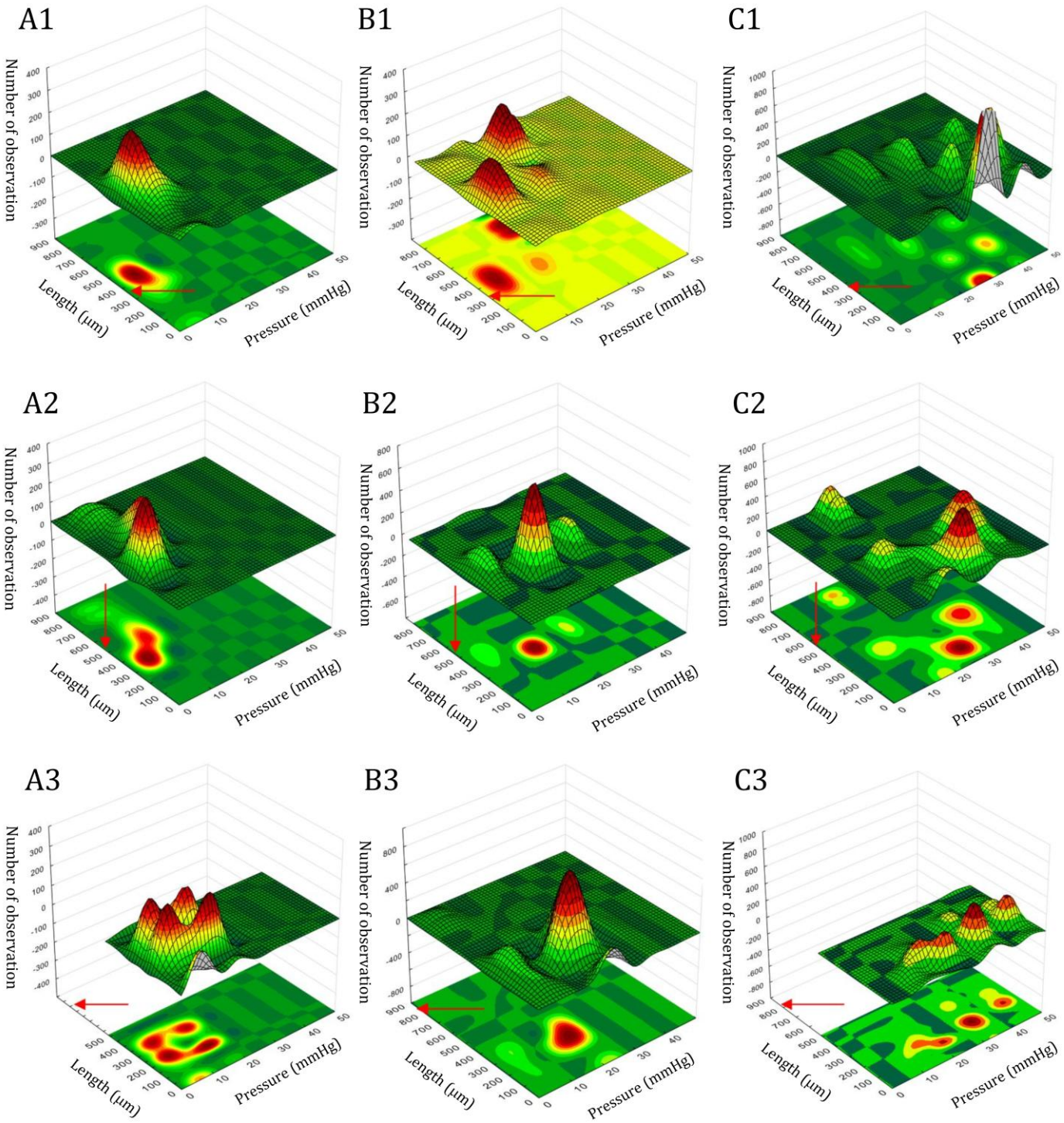

Fig. 5 Distribution of the lengths of air bubbles versus applied air pressures (similar to those used in gastroscopy) on channels with perforated walls, for perforations with 16 μm widths (A column), 32 μm widths (B column), and 100 μm widths (C column), into artificial blood vessels with widths of 30 μm (first row), 50 μm (second row), and 80 μm (third row). Note the decreasing presence of bubbles longer than the distance between the bifurcations (indicated by red arrows, 311 μm, 519 μm, and 830 μm, for vessels widths of 30 μm, 50 μm, and 80 μm, respectively) from small vessels and small perforations (mostly evident in A1, B1, and A2) to absence in large vessels and large perforations (mostly evident in A3, B3, and C3).

(ii). Conversely, in larger vessels (80 μm and 250 μm, with an inter-bifurcation distance of 2.6 mm, not presented in Fig. 5) the ends of the Taylor air bubbles remained below the distance separating two consecutive bifurcations.

C2. Mimicking carbon dioxide gas embolism. In contrast with air, carbon dioxide did not produce discrete individual bubbles. Instead, distinct gas-liquid flow patterns emerged (or near-infinite Taylor bubbles), once the pressure of carbon dioxide exceeded a geometry-specific threshold (Fig. 6). These patterns included (i) parallel gas and liquid flow (Movie SI.1), (ii) alternating gas and liquid flow (Movie SI.2), and (iii) channel Blockage by gas (Movie SI.3).

The geometry of the microvasculature, namely the channel width to perforation size ratio, was the key factor governing the observed flow regimes. Ratios higher than 2.5 (denoted pink in Fig. 6) resulted in parallel flow, while low ratios (below 0.5; orange) led to channel blockage. Intermediate geometries produced alternating gas and liquid flow. In these cases, continuous gas intrusion events typically lasted between 3 and 40s. However, sporadic gas bursts of up to 1650s highlighted the unpredictable nature of carbon dioxide embolism events.

The threshold pressure required for carbon dioxide entry into the vascular channel ranged from 23 ± 4 to 58 ± 6 mm Hg (Fig. 6). No statistically significant differences existed among channel width-perforation size combinations. The only exception involved the smallest perforations (16 µm), where 50-250 µm wide channels required significantly higher pressures to initiate gas entry – up to 1.8 times larger than those measured for equivalent channels with larger perforations.

The carbon dioxide-specific alternating liquid and gas flow led to the gas filling the space between two bifurcations sites within three seconds, irrespective of the geometric configuration.

D. Scenario 2. Percolation of Gas through Physically Intact Walls of Blood Vessels

D1. Air percolation through intact walls. Vessel thickness of 75 µm did not lead to any apparent air transfer into the liquid phase, irrespective of the applied pressure. At the opposite extreme, channels with 25 µm-thick walls consistently experienced mechanical failure at low pressures in repeated trials, resulting in wall rupture, and subsequent direct gas injection into the vascular channel. However, while the intermediate 50 µm-thick walls remained physically intact, they allowed the percolation of air in the form of bubbles (also observed elsewhere [78]).

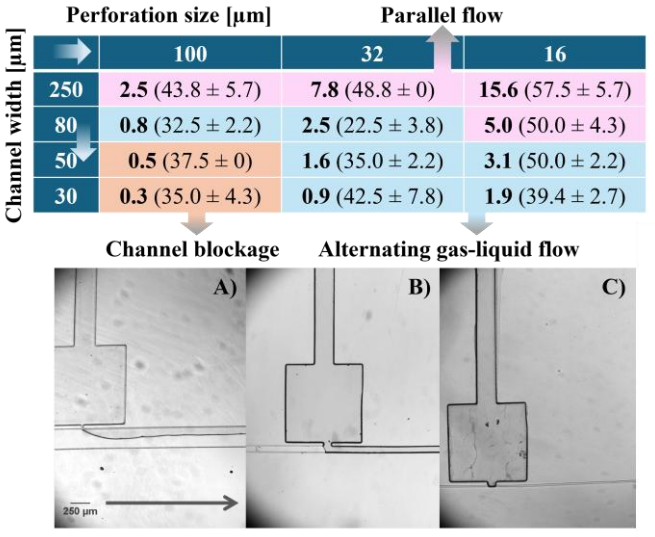

Fig. 6 Channel width to perforation size ratios, corresponding threshold pressures of carbon dioxide, and their translation into flow patterns of carbon dioxide: (A) parallel flow, (B) alternating gas-liquid flow, (C) channel blockage. The arrowhead represents flow direction.

For all channel widths investigated, increasing air pressure resulted in a corresponding increase in the average bubble volume. The increase followed an approximately logarithmic relationship with the applied pressures, with the largest bubbles appearing in the 250 µm-wide channels, primarily due to bubble coalescence (Fig. SI.1).

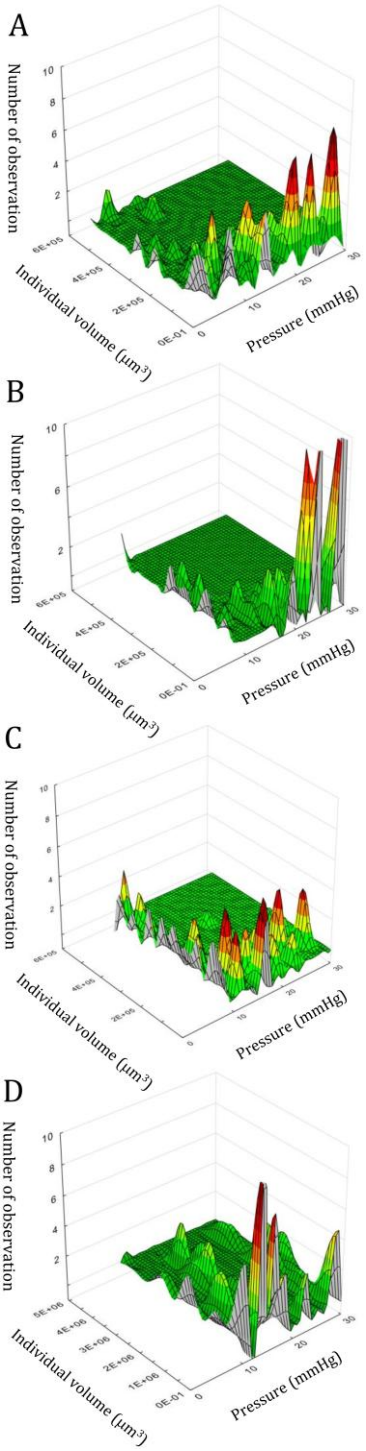

Fig. 7 Distribution of volumes of air bubbles versus applied pressures (similar to those in gastroscopy) in channels without perforated walls, for widths of the artificial blood vessels of 30 µm (A), 50 µm (B), 80 µm (C), and 250 µm (D). Circles indicate a sizable minority of larger bubbles at lower pressures.

A more detailed analysis of the volumes of individual bubbles, modulated by the applied pressure, revealed several characteristic trends (Fig. 7):

(i). Regardless of the channel width, the largest proportion of bubbles have small volumes.

(ii). Similarly to their perforated counterparts, 30-80 µm-wide channels exhibited a sizable minority of relatively large bubbles, especially at lower pressures (circles in A-C in Fig. 7).

(iii). The pressure threshold at which bubbles begin to appear through percolation increases from small to large widths of the blood vessels (A to D in Fig. 7).

Importantly, the frequency of the genesis of air bubbles via percolation through intact blood vessels walls is approximately two orders of magnitude lower than that via transfer through calibrated perforations (number of observations in Fig. 4, and Fig. 7, respectively). In addition, the volume of the bubbles via percolation are substantially smaller than those obtained via transfer through calibrated perforations.

D2. Carbon dioxide percolation through intact walls. Mechanical stability of the channel wall is governed primarily by its structural, rather than gas-specific properties. Therefore, the carbon dioxide experiments focused exclusively on devices with 50 µm-thick walls, where gas embolism events were observed when using air. Unlike air, carbon dioxide did not produce detectable gas transfer into the vascular channel. No bubble formation, continuous gas injection or other embolism-like events were observed for applied pressures of up to 150 mm Hg, independent of channel width.

D3. Comparison of the rates of generation of air bubbles. An analysis of the generation rates of air bubbles through calibrated perforations (Scenario 1) and through intact thin walls (Scenario 2), separate from the previous analysis of individual volumes (Fig 4 and 7), provides additional insights into the likelihood of gas embolism at the microscale. Similarly with the size of individual bubbles, the rate of creation of air bubbles through percolation (Fig 8A) is approximately two orders of magnitude lower than the rates observed for the transfer though calibrated perforations (Fig. 8B, 8C, and 8D). In addition, notwithstanding the large differences in total volumes, the rate of air injected via percolation through an intact wall and for small perforations (16 µm and 32 µm) is increasing for larger widths of the blood vessels *and* applied pressure (Fig 8A, 8B, and 8C, respectively). In contrast, for large perforations (100 µm, Fig 8D) the rate of air injections is rather independent on both vessel size and applied pressure. Interestingly, for Scenario 1, the certainty of the correlation rate of injection and pressure decreases near-linearly with the increase of the ratio between the perforation size and width of the vessel (Table SI.2 and Fig. SI.3). This observation underlines the more chaotic character of the genesis of emboli for large perforations.

D4. Different patterns of air and carbon dioxide gas embolism at microscale. One important observation of the present study consists in the distinct patterns of air, and carbon dioxide gas embolism, i.e., rapid onset and large population of bubbles with various volumes depending on applied pressure and microvasculature geometry for air embolism; and delayed onset and very large or continuous Taylor bubbles for carbon dioxide embolism. The delayed production of bubbles when carbon dioxide is used can be explained by its high solubility compared with that of air, leading to the liquid phase acting as a 'sink', absorbing the carbon dioxide until an equilibrium concentration is reached in bulk, or until this concentration is reached at the surface of the liquid delaying further diffusion inside. When this threshold is reached the surface tension of the liquid will change. The low solubility of air translates into low

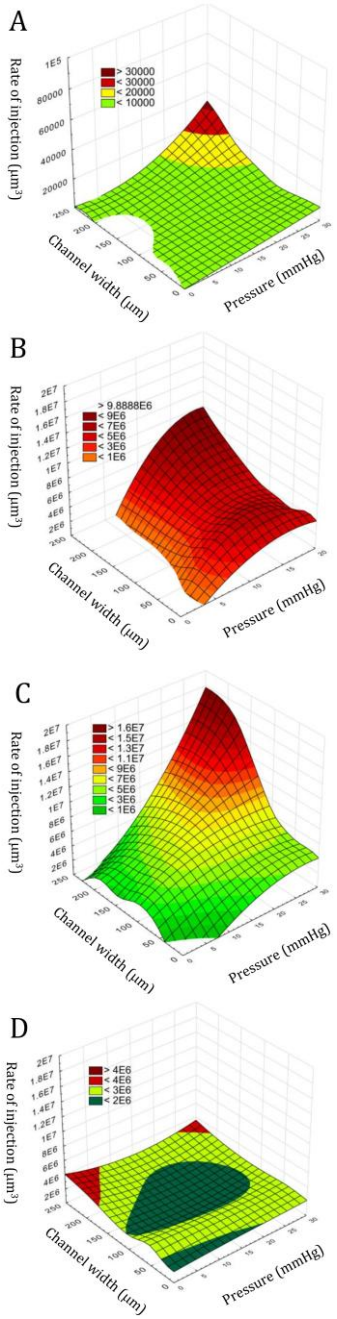

Fig. 8. Rate (µm³/s/blood vessel) of production of air bubbles through percolation (A) and injection through calibrated perforations of 16 µm, 32 µm, and 100 µm (B, C, D) versus channel width and applied pressure.

concentration in blood, and consequently negligible changes in the surface tension of blood, and consequently its unchanged surface tension. In contrast, the high (and likely rapid) uptake of carbon dioxide will change liquid properties, especially at the interface with gas. While pure water has a surface tension of 71 mN/m, carbon dioxide-saturated water presents a surface tension of 65 mN/m at atmospheric pressure (lower at higher pressures)[79]. Admittedly, the surface pressure of blood is considerably lower, at approximately 56 mN/m [80, 81] which would be further lowered by the uptake of carbon dioxide to approximately 51 mN/m (assuming a linear decrease similar to that of water). A lower surface tension of carbon dioxide-saturated fluid will lead to larger bubbles. Indeed, it was demonstrated [82] that the decrease of surface tension the liquid

leads to a linear increase of the volume of gas bubbles from 6 to 15%. Consequently, these larger bubbles confined in narrow confining blood vessels will result in long Taylor bubbles. Finally, while the artificial blood is salt-free, salts are present in real blood, further reducing surface tension[80].

The characteristics of the carbon dioxide gas embolism, i.e., Taylor bubbles longer than the field of the optical field of view, or 'infinite' bubbles (gas flowing in parallel with the fluid) suggest that these bubbles are longer than any distance between bifurcation of the blood vessels studied. Also, these characteristics made impossible an analysis similar to that performed for air embolism at the microscale.

E. Scenario 3. Ex-diffusion from Supersaturated Tissues

E1. Degassing artificial tissues. PDMS chips were stored for several hours in ambient conditions prior experiments, reaching equilibrium concentration of gas at atmospheric pressure. When higher pressures, similar to those used in laparoscopy and gastroscopy, were applied in the adjacent pressure chamber, bubbles rapidly formed in the blood vessels even through non-perforated channels (Fig. 9A, upper row, Movies SI.4-5), as described above. In contrast, no bubbles emerged in channels if the chips were previously subjected to vacuum degassing (Fig. 9A, middle and bottom row, Movies SI.6-8).

The absence of bubbles when surrounding material is depleted of dissolved gases, even if the artificial microvasculature is subsequently exposed to higher air pressures, can be explained by gas-depleted PDMS acting as a 'sink' for the gas, until an equilibrium is reached, after which thin membrane-mediated transfer in gas-saturated blood. This experiment is a control to demonstrate the role of the level of the concentration in the surrounding tissue prior, during, and after gas embolism events.

E2. Saturation of artificial tissues with nitrogen. Conversely, when the surrounding artificial tissue was super-saturated with nitrogen at high pressure, bubbles appeared immediately in the liquid phase upon exposure to normal pressure (Fig. 9B, Movies SI.9–14). Notably, bubble formation persisted for up to 1.5 h after operation at atmospheric pressure (Movies SI.15–16). While nitrogen served as a conservative model gas due to its lower solubility limiting overall gas uptake, these findings indicate that the artificial tissue can act, in principle, as a transient gas reservoir, delaying the dissolution of air bubbles after the initial pressurization phase ended, consistent with a delayed release mechanism (Scenario 3).

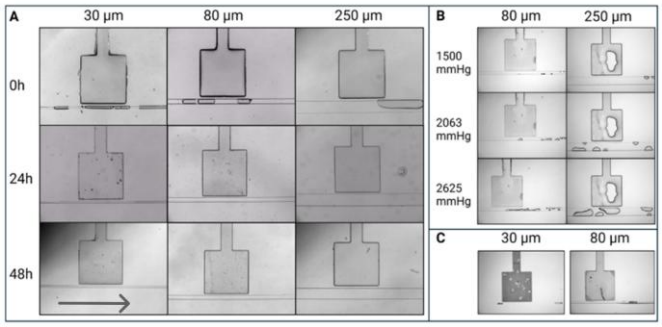

Fig. 9 Comparison of bubble generation in microfluidic devices presented to various storage conditions. A. Absence of bubbles in devices that were degassed for 24 and 48 hours, even if air pressure at 15.5 mmHg was applied in the pressure cavity. B. Presence of bubbles in devices first degasified for 48 hours, followed by an immersion in nitrogen for 48 hours at various pressures. C. Appearance of bubbles in channels with 30 µm and 80 µm widths, 1.5 hours after the previous immersion in nitrogen, followed by a return to atmospheric conditions. The arrowhead indicates the flow direction. Note that while the pressures used for the saturation of the artificial tissue with gas are considerably higher than those in laparoscopy and gastroscopy, they are within the ranges of the maximum pressure of many naval hyperbaric protocols.

E3. Tissue saturation with carbon dioxide. Subjecting the artificial tissue to carbon dioxide at 1500 mm Hg was sufficient to induce subsequent bubble formation within the vascular channels (Movies SI.17–19, Fig 9, Fig SI.2). While carbon dioxide saturation experiments do not have medical relevance, they demonstrate the role of surround tissues in acting as 'reservoirs' for gas 'leaking' in the blood stream.

E4. Mechanism of ex-diffusion from gas-saturated tissues. These results are likely to reflect a balance between two competing processes: removal of dissolved carbon dioxide by convective liquid flow and replenishment of gas from surrounding saturated material. Importantly, in addition to tissue-level storage effects, the PDMS-based experiments demonstrate a distinct transport pathway in which gas can traverse an intact barrier separating a pressurized gas environment from a perfused microchannel. The absence of bubble formation following PDMS degassing indicates that the gas reaching the channel originates from gas stored within and transported through the PDMS matrix under an applied pressure gradient. This behavior is consistent with gas transport across physically intact vascular walls as described in Scenario 2. The present experiments do not allow direct determination of whether gas reaches the microchannel in the gaseous phase or whether it first dissolves into the liquid phase and subsequently nucleates due to local pressure variations. Such pressure gradients along the microchannel may reduce gas solubility and promote bubble formation from a saturated or supersaturated solution. Therefore, while nucleation may contribute to the final appearance of bubbles, the results support the existence of a trans-barrier gas transport rather than a specific phase transition pathway during transport. The intermediate channel width appears to provide the most effective washout of dissolved gas while maintaining a relatively limited gas-exchange surface area, further highlighting the interplay between convective removal and barrier-mediated gas transport.

F. Medical Significance

The near physical-only nature of gas embolism during its earliest stages justified the investigation using abiotic microfluidic systems mimicking key aspects of *in vivo* systems, i.e., dimensions of blood vessels, pressure conditions, fluid rheology, and mechanical properties of tissue. Consequently, and notwithstanding the relatively low reported incidence of gas embolism in endoscopic procedures (0.57 per 100,000 endoscopic procedures) [83], the extrapolation of the experimental results presented here suggest possible insights or areas of future studies with practical medical relevance.

F1. Time of gas injection to reach dangerous levels in human body. The reported lethal dose of intravascular air is approximately 3-5 mL/kg[84], corresponding to an estimated lethal volume of 240 mL for a 60 kg patient, when adopting a mean value of 4 mL/kg. Reaching this lethal volume would take 8-12 s at the insufflation rates used during gastroscopy, assuming perfectly efficient injection of gas into the circulation. The situation is more complex for carbon dioxide because of its approximately 20 times greater solubility in blood[85]. In this

context, an experimental study in pigs reported mortality rates of 60% following arterial carbon dioxide injection at 1.2 mL/kg/min[86]. To put things in context, for a 60 kg patient, this lethal flow rate corresponds to a gas delivery rate approximately four times lower than the mean maintenance flow rate used during laparoscopy. Even accounting for lower real gas transfer efficiency, these estimates still illustrate that clinically significant embolism could develop rapidly, allowing only limited time for medical detection and intervention. Consequently, the implementation of continuous measurement and automatic regulation of gas pressure *and* flow rate used in endoscopic procedures, also associated with warning signaling and emergency intervention, appear warranted.

F2. Gas embolism initiated through calibrated perforations (Scenario 1). The experimental results suggest that:

(i). In general, the balance between vascular and external gas pressure determines if vascular injury results in bleeding or in gas intake in blood vessels. Whenever external gas pressure sufficiently exceeds blood pressure, gas intake becomes favorable. This condition is particularly relevant in venules, where pressures typically range between 8-12 mm Hg[87] and may approach 0 mm Hg in the smallest vessels[88, 89].

(ii). Air embolism-like events developed over a pressure range that largely overlaps with reported gas pressures used gastroscopy (approximately 5-60 mm Hg; Fig. 4). Importantly, a significant fraction of gas embolism events occurs below the officially reported maximum level of 20 mm Hg, indicating that gas entry may occur under routine operating conditions, with accidental over-pressurization not necessary (Fig. 3).

(iii). Air embolism bellow 20 mm Hg is particularly concerning in vessels representative of arterioles and venules within the esophageal lining (30-80 μm-wide)[90] with small perforations (16 μm). While the rate of gas injection is small, it could proceed unnoticed given the small scale of the vessels and perforations, thereby enabling gradual accumulation or aggregation of emboli within blood circulation. Such silent progression would pose significant risks as it delays intervention until already critical clinical symptoms occur.

(iv). Larger blood vessels (250 μm-wide) affected by pre-existing pathology may exhibit elevated intravascular pressures. This situation is particularly relevant in patients with a liver disease or scarring who undergo therapeutic gastroscopy for the treatment of sclerotic or actively bleeding esophageal varices. Although intravascular pressures in these vessels may exceed normal physiological values, they remain within the range of pressures reported in gastroscopy. Consequently, the pressure gradient may still favor air entry into the circulation. Owing to their larger cross-sectional area, these vessels can also permit substantially higher rates of gas injection. Importantly, gas entry into the vessel may reduce or temporarily stop visible bleeding – the intended outcome of the therapeutic intervention – thereby masking the onset of air embolism. This mechanism could be responsible for another path of 'silent' air embolism, in which large volumes of air can enter the blood circulation without overt clinical signs.

(v). An important observation specific to air embolism is the formation of a sizable minority of larger bubbles at low pressures, translating in an increased risk of complete vascular blockage, in contrast with many, but small bubbles at larger pressures. These findings challenge the common assumption that larger bubbles are exclusively associated with higher insufflation pressures. Indeed, although lower insufflation pressures are generally recommended in clinical practice, with 10 mm Hg often regarded as a 'safe' operating pressure [91], the present results suggest that low-pressure insufflation does not necessarily eliminate the risk of generating large emboli.

(vi) Carbon dioxide embolism required higher threshold pressures, i.e., 32.5-57.5 mm Hg, depending on the combination of blood vessel width/wall perforation. Although these values exceed standard laparoscopic operating pressures (10-20 mm Hg), they represent only a modest increase of up to 8% in absolute pressures, which can result from pressure fluctuations, equipment malfunction, or procedural events (Fig. 3). For example, trocar insertion was reported to transiently increase intra-abdominal pressure by 18-23 mm Hg[74].

(vii). An additional concern associated with carbon dioxide embolism arises from its distinct gas-liquid flow patterns. In contrast to the discrete bubbles, characteristic to air embolism, the alternating gas-liquid flow, and to a lesser extent the parallel flow, are considerably more hazardous events, which could lead to much greater volumes of injected carbon dioxide. Consequently, while carbon dioxide-related embolism events occur, in abiotic mimicking systems at higher pressures, once triggered, they lead to more extensive gas exposure and potentially more severe physiological consequences. This increased severity is reflected in the prolonged interruption of liquid flow, with gas occupying the vessel for 13-95% of the observation period, as well as in the rapid propagation of gas through the microvascular network. In all cases of alternating gas-liquid flow, carbon dioxide traversed the equivalent distance between two consecutive bifurcations in less than 3s.

F3. Gas embolism through thin vessel wall (Scenario 2).

(i). Blood vessels with wall thickness below 25 μm, representative of small venules and arterioles, are susceptible to localized micrometer-scale ruptures when directly exposed to pressurized gas. The ruptures occur independently of the insufflation gas, i.e., air or carbon dioxide, because their main cause is mechanical failure. Therefore, and depending on the pressure balance, the relevance of pressure induced wall breakage is relevant, in principle, to both laparoscopy and gastroscopy. In contrast, undamaged blood vessels with walls thicker than 75 μm appear to be resilient against microscopic gas embolism events.

(ii). Blood vessels with intermediate wall thickness (50 μm) exhibit gas-dependent behavior of mass transfer. When exposed to pressurized air, intravascular bubbles are rapidly developed despite the absence of visible wall damage. In contrast, exposure to carbon dioxide at comparable or higher pressures (up to 100 mm Hg) does not induce detectable gas embolism events. These findings are consistent with the adverse outcomes reported for air-based gastroscopy, including symptomatic gas embolism with severe neurological complications[62]. Collectively, the results support further investigation into the use of carbon dioxide as an alternative insufflation gas during gastroscopy aiming to reduce the risk of embolism.

(iii). The patterns of air embolism in non-perforated vasculature are similar to those in injured vessels. First, air bubbles form at low pressures, used in gastroscopy, in 30-80 μm-wide blood vessels. Second, a small but distinct population of large bubbles emerged at low pressure (Fig. 7) [81].

F4. Lengths of gas emboli in blood vessels with various widths.

(i). Behavior of an air emboli situated at microvascular bifurcations may contribute to a second tier of gas embolism events. Upon reaching a bifurcation, a bubble may lodge, obstruct blood flow and reduce the convective transport that promotes gas dissolution. Alternatively, the bubble can fragment and propagate into downstream branches, distributing the embolic burden throughout the microvascular network and initiating additional sites of vascular obstruction[81].

(ii). When using carbon dioxide, the alternating gas-liquid flow regime inherently results in gas occupying the entire distance between consecutive bifurcations once the pressure threshold for embolism is met. Furthermore, if the gas front propagates into both daughter vessels, bifurcation-induced splitting may not immediately accelerate gas dissolution because the resulting gas segments remain substantially larger than the discrete air bubbles observed under comparable conditions. Consequently, despite the higher solubility of carbon dioxide, extensive gas occupation of the microvascular network may still lead to significant and sustained flow disruption at the microscale.

From a medical perspective, it must be noted that, although the physical mechanism of percolation was demonstrated here, the bubbles generated are unlikely to pose a critical risk for gas embolism, due to their orders of magnitude lower frequency, considerably reduced volume compared with bubbles generated via transfer through perforations in the blood vessel walls, and the limitations imposed by the very thin wall of the blood vessels, i.e., around 50 μm.

F5. Impact of gases dissolved in tissues (Scenario 3).

(i). Following saturation of the artificial tissue with nitrogen, a gas characterized by low solubility in PDMS, bubbles formed immediately in freshly introduced, non-saturated artificial blood upon return to atmospheric pressure. Notably, bubble generation persisted for up to 1.5 h during storage under ambient conditions. The saturation experiments were run at considerably higher pressures than those used in laparoscopy and endoscopy, thus limiting their relevance for these medical procedures. However, the pressures used in gas saturation experiments, i.e., relative pressure of 1500-2600 mm Hg (3 to 4.4 atm absolute pressure), are similar to the maximum pressures used in several U.S. Navy Treatment Tables, e.g., 1.8 atm for USN TT4 to 5 atm for USN TT6 [92], during which the patients are exposed to air or an alternation of air and oxygen for 75 min to 2 hrs. These observations demonstrate the ability of the tissues to act as gas reservoirs, sustaining bubble formation in previously unsaturated blood long after the initial gas embolism event ended or following apparent clearance of intravascular bubbles. This delayed release mechanism has important clinical implications. Specifically, this mechanism suggests that residual gas stored in tissues may continue to pose an embolic risk even after conventional indicators suggest resolution of the acute event. Consequently, extending the duration of hyperbaric oxygen therapy (HBOT) beyond the apparent disappearance of circulating bubbles appears as warranted. A reported case of gastroscopy-related air embolism supports this interpretation as the patient's condition improved progressively over three HBOT sessions administered over a total period of 48 h[62].

(ii). Tissue saturation experiments with carbon dioxide mimicked the situation in laparoscopic surgery, i.e., (i) tissue initially equilibrated with ambient air, (ii) then subjected to pressurized carbon dioxide for 30 min, (iii) washed with fresh artificial blood in the absence of external gas pressure. The immediate appearance of carbon dioxide bubbles upon perfusion indicates that clinically relevant durations of pressure exposure could be sufficient to establish tissue reservoirs containing enough dissolved carbon dioxide to supersaturate circulating blood and induce bubble formation. Moreover, the experiments demonstrated that smaller blood vessels with lower blood flow rates were more susceptible to bubble formation at the microscale. These blood vessels are more likely to be in proximity to saturated tissues, increasing the probability of carbon dioxide being released into the bloodstream. From a medical perspective, the competition between the uptake of carbon dioxide in tissues faster than for air, leading to high concentrations in short times, counterbalanced by the quick transfer in blood, suggests further research directions in abiotic microfluidic systems.

IV. CONCLUSION

This study presented a microfluidic platform for *in vitro* study of the genesis of gas embolism at microscale arising from invasive medical procedures involving pressurized gases. Air and carbon dioxide, across clinically relevant pressure ranges, served as representative gases used in gastroscopy and laparoscopy, respectively.

The results suggest that air embolism could occur at pressures routinely employed during gastroscopy. While ruptures of 25 μm-thick vascular walls occurred, air bubbles entered the circulation even through intact walls of blood vessels of 50 μm thickness. Importantly, a sizable minority of larger bubbles form at relatively low pressures. Larger emboli are of particular concern because of their slower dissolution rates and greater likelihood of becoming lodged within blood vessels. Bubble formation and vascular entry increased in vessels with perforations mimicking legions, while maintaining the same characteristic of a sizable minority of large emboli. These findings highlight the need for improved pressure *and* gas flow rate monitoring in gastroscopy, where insufflation is currently performed according to operator's experience. The rapid passage of gas into damaged vessels underscores the importance of thorough vascular assessment prior therapeutic gastroscopy, which frequently involve active bleeding sites.

Carbon dioxide embolism developed at pressures only modestly exceeding those typically used in laparoscopy. Additionally, carbon dioxide embolism exhibited a more abrupt onset and higher gas volumes entering the circulation. These observations suggest that the risk of carbon dioxide embolism during laparoscopy may be underestimated and warrants increased clinical awareness.

Supersaturated tissues appear to act as gas 'reservoirs', potentially prolonging gas embolism after therapy. Suggesting that further research is needed to assess the optimum protocols for hyperbaric oxygen therapy.

V. Acknowledgment

We thank Prof. David Eckmann from Ohio State University for insightful discussions.

References

[1] S. Gordy and S. Rowell, "Vascular air embolism," *Int. J. Crit. Illn. Inj. Sci.*, vol. 3, no. 1, pp. 73–76, Jan. 2013.
[2] S. Goldman, J. M. Solano-Altamirano, and K. M. LeDez, *Gas Bubble Dynamics in the Human Body*. Cambridge, MA, USA: Academic Press, 2017.
[3] A. Bettiol *et al*., "Erythrocyte oxidative stress and thrombosis," *Expert Rev. Mol. Med.*, vol. 24, Art. no. e31, Dec. 2022.
[4] L. O. Ferreira *et al*., "Biochemical changes in cardiopulmonary bypass in cardiac surgery: New insights," *J. Pers. Med.*, vol. 13, no. 10, Art. no. 1506, Oct. 2023.
[5] W. Fan *et al*., "A narrative review on lung injury: Mechanisms, biomarkers, and monitoring," *Crit. Care*, vol. 28, Art. no. 280, 2024.
[6] . M. Auñón-Chancellor *et al*., "Venous thrombosis during spaceflight," *N. Engl. J. Med.*, vol. 382, no. 1, pp. 89–90, Jan. 2020.
[7] Y. Y. Phillips, "Primary blast injuries," *Ann. Emerg. Med.*, vol. 15, no. 12, pp. 1446–1450, Dec. 1986.
[8] C. Horrocks, "Blast injuries: Biophysics, pathophysiology and management principles," *J. R. Army Med. Corps*, vol. 147, no. 1, pp. 28–40, Apr. 2001.
[9] A. M.-H. Ho and E. Ling, "Systemic air embolism after lung trauma," *J. Am. Soc. An.*, vol. 90, no. 2, pp. 564–575, 1999.
[10] K. M. LeDez, "Air embolism and blunt chest trauma," *Can. J. Anaesth.*, vol. 58, no. 12, pp. 1140–1141, Dec. 2011.
[11] Y. Hashimoto *et al*., "Cerebral air embolism caused by cardiopulmonary resuscitation after cardiopulmonary arrest on arrival," *J. Trauma*, vol. 48, no. 5, pp. 975–977, May 2000.
[12] L. M. Bralow and M. Piehl, "Barotrauma and arterial gas embolism: A diving emergencies simulation case for emergency medicine residents," *MedEdPORTAL*, vol. 14, Art. no. 10788, Dec. 2018
[13] D. Riley *et al*., "World Trade Center terror: Explosion trauma—blast, burns, and crush injury," *Adv. Emerg. Nurs. J.*, vol. 24, no. 2, pp. 47–59, 2002
[14] Y. Mushkat *et al*., "Gas embolism complicating obstetric or gynecologic procedures: Case reports and review of the literature," *Eur. J. Obstet. Gynecol. Reprod. Biol.*, vol. 63, no. 1, pp. 97–103, Nov. 1995
[15] C. M. Muth and E. S. Shank, "Gas embolism," *N. Engl. J. Med.*, vol. 342, no. 7, pp. 476–482, Feb. 2000
[16] P. L. Marsh *et al*., "Iatrogenic air embolism: Pathoanatomy, thromboinflammation, endotheliopathy, and therapies," *Front. Immunol.*, vol. 14, Art. no. 1230049, Sep. 2023
[17] C. J. McCarthy *et al*., "Air embolism: Diagnosis, clinical management and outcomes," *Diagnostics*, vol. 7, no. 1, Art. no. 5, Jan. 2017.
[18] N. Heming *et al*., "Update on the management of iatrogenic gas embolism," in *Annual Update in Intensive Care and Emergency Medicine 2020*, J.-L. Vincent, Ed. Cham, Switzerland: Springer Int. Publ., 2020, pp. 559–568.
[19] S. Q. Liu *et al*., "Monitoring of gas emboli during hysteroscopic surgery: A prospective study," *J. Ultrasound Med.*, vol. 36, no. 4, pp. 749–756, Apr. 2017
[20] V. Červeňák *et al*., "Cerebral air embolism: Neurologic manifestations, prognosis, and outcome," *Front. Neurol.*, vol. 15, Art. no. 1417006, 2024
[21] A. M. Alexander *et al*., "Arterial gas embolism," in *StatPearls* [Online]. Treasure Island, FL, USA: StatPearls Publishing, 2024. Available: https://www.ncbi.nlm.nih.gov/books/
[22] E. J. Thomas *et al*., "Case report: Management of cerebral arterial gas embolism via transfer to an outpatient hyperbaric chamber," *Front. Med.*, vol. 12, Art. no. 1533459, Apr. 2025
[23] S. Fuentes *et al*., "Gas embolism in pediatric minimally invasive surgery: Should it be a concern?," *J. Laparoendosc. Adv. Surg. Tech. A*, vol. 33, no. 10, pp. 1011–1017, Oct. 2023.
[24] R. E. Moon, "Arterial gas embolism," *Merck Manual Professional Edition*. Accessed: 2023. [Online]. Available: https://www.merckmanuals.com/en-ca/professional/injuries-poisoning/injury-during-diving-or-work-in-compressed-air/arterial-gas-embolism
[25] K. Baassiri *et al*., "In vitro studies of gas embolism," in *Recent Advances in Hemodynamics and Blood Mimetics*, J. M. R. Miranda, A. S. O. H. Moita, T. Fukui, Z. Ostrowski, and R. A. M. M. Lima, Eds. Amsterdam, The Netherlands: Elsevier, 2025, pp. 313–344
[26] D. Hatling *et al*., "Iatrogenic cerebral gas embolism—A systematic review of case reports," *Acta Anaesthesiol. Scand.*, vol. 63, no. 2, pp. 154–160, Feb. 2019.
[27] Z. U. Rahman *et al*., "Cardiac arrest as a consequence of air embolism: A case report and literature review," *Case Rep. Med.*, vol. 2016, Art. no. 8236845, 2016
[28] T. Wu *et al*., "Two cases of fatal iatrogenic air embolism confirmed by autopsies," *J. Forensic Leg. Med.*, vol. 82, Art. no. 102209, 2021.
[29] M. M. Mardanpour *et al*., "Gas embolism: Fundamentals, diagnosis, and treatment," *IEEE Rev. Biomed. Eng.*, early access, pp. 1–18, 2026
[30] P. Mandelstam *et al*., "Complications associated with esophagogastroduodenoscopy and with esophageal dilation," *Gastrointest. Endosc.*, vol. 23, no. 1, pp. 16–19, 1976.
[31] L. K. Afreen *et al*., "Incidence of venous air embolism during endoscopic retrograde cholangiopancreatography," *Anesth. Analg.*, vol. 127, no. 2, pp. 420–423, Aug. 2018.
[32] M. Derouin *et al*., "Detection of gas embolism by transesophageal echocardiography during laparoscopic cholecystectomy," *Anesth. Analg.*, vol. 82, no. 1, pp. 119–124, Jan. 1996.
[33] E. Y. Park *et al*., "Carbon dioxide embolism during laparoscopic surgery," *Yonsei Med. J.*, vol. 53, no. 3, pp. 459–466, May 2012.
[34] T. M. Atkinson *et al*., "Cardiovascular and ventilatory consequences of laparoscopic surgery," *Circulation*, vol. 135, no. 7, pp. 700–710, Feb. 2017.
[35] Q. Wu *et al*., "Organ-on-a-chip: Recent breakthroughs and future prospects," *Biomed. Eng. Online*, vol. 19, Art. no. 9, 2020.
[36] Y. Lu *et al*., "Adhesion of silicone oil and emulsification: An in vitro assessment using a microfluidic device and 'Eye-

on-a-Chip'," *Acta Ophthalmol.*, vol. 97, no. 3, pp. 313–318, May 2019.
[37] A. Verma and M. P. Singh, "Venous gas embolism in operative hysteroscopy: A devastating complication in a relatively simple surgery," *J. Anaesthesiol. Clin. Pharmacol.*, vol. 34, no. 1, pp. 103–106, Jan.–Mar. 2018.
[38] J. Bazin *et al*., "Haemodynamic conditions enhancing gas embolism after venous injury during laparoscopy: A study in pigs," *Br. J. Anaesth.*, vol. 78, no. 5, pp. 570–575, May 1997.
[39] J. J. Maleszewski *et al*., "Anatomic considerations and examination of cardiovascular specimens (excluding devices)," in *Cardiovascular Pathology*, 5th ed., L. T. Cooper and J. P. Veinot, Eds. Philadelphia, PA, USA: Elsevier, 2022, pp. 27–84.
[40] K. R. Olson, "Physiology of capacitance vessels," in *Encyclopedia of Fish Physiology*, A. P. Farrell, Ed. San Diego, CA, USA: Academic Press, 2011, pp. 1111–1118.
[41] L. Si *et al*., "A human-airway-on-a-chip for the rapid identification of candidate antiviral therapeutics and prophylactics," *Nat. Biomed. Eng.*, vol. 5, no. 8, pp. 815–829, Aug. 2021.
[42] M. Zhang *et al*., "Biomimetic human disease model of SARS-CoV-2-induced lung injury and immune responses on organ chip system," *Adv. Sci.*, vol. 8, no. 3, Art. no. 2002928, Feb. 2021.
[43] D. Huh *et al*., "Reconstituting organ-level lung functions on a chip," *Science*, vol. 328, no. 5986, pp. 1662–1668, Jun. 2010.
[44] T. Cao *et al*., "Biomimetic alveolus-on-a-chip for SARS-CoV-2 infection recapitulation," *Research*, vol. 2022, Art. no. 9819154, 2022.
[45] B. Müller *et al*., "High-resolution tomographic imaging of microvessels," in *Proc. SPIE Developments in X-Ray Tomography VI*, vol. 7078, 2008, pp. 89–98.
[46] T.-Y. Tu and P. C.-P. Chao, "Continuous blood pressure measurement based on a neural network scheme applied with a cuffless sensor," *Microsyst. Technol.*, vol. 24, pp. 4539–4549, Nov. 2018.
[47] B. Alberts *et al*., "Blood vessels and endothelial cells," in *Molecular Biology of the Cell*, 4th ed. New York, NY, USA: Garland Science, 2002.
[48] E. Nader *et al*., "Blood rheology: Key parameters, impact on blood flow, role in sickle cell disease and effects of exercise," *Front. Physiol.*, vol. 10, Art. no. 1329, 2019.
[49] L. Webb, "Mimicking blood rheology for more accurate modeling in benchtop research," *Pegasus Rev.: UCF Undergrad. Res. J.*, vol. 12, no. 1, Art. no. 6, 2020.
[50] K. Brookshier and J. Tarbell, "Evaluation of a transparent blood analog fluid: Aqueous xanthan gum/glycerin," *Biorheology*, vol. 30, no. 2, pp. 107–116, 1993.
[51] T. E. Kornfield and E. A. Newman, "Measurement of retinal blood flow using fluorescently labeled red blood cells," *eNeuro*, vol. 2, no. 2, Art. no. ENEURO.0005-15.2015, 2015.
[52] E. L. Jablonski *et al*., "Microfluidics in the undergraduate laboratory: Device fabrication and an experiment to mimic intravascular gas embolism," *Chem. Eng. Educ.*, vol. 44, no. 1, pp. 81–87, 2010.
[53] A. B. Schroeder *et al*., "The ImageJ ecosystem: Open-source software for image visualization, processing, and analysis," *Protein Sci.*, vol. 30, no. 1, pp. 234–249, Jan. 2021.
[54] G. Arthurs and M. Sudhakar, "Carbon dioxide transport," *Contin. Educ. Anaesth. Crit. Care Pain*, vol. 5, no. 6, pp. 207–210, Dec. 2005.
[55] C. Henny and J. Hofland, "Laparoscopic surgery: Pitfalls due to anesthesia, positioning, and pneumoperitoneum," *Surg. Endosc.*, vol. 19, pp. 1163–1171, Sep. 2005.
[56] M. Perrin and A. Fletcher, "Laparoscopic abdominal surgery," *Contin. Educ. Anaesth. Crit. Care Pain*, vol. 4, no. 4, pp. 107–110, Aug. 2004.
[57] X. Yang *et al*., "Gases for establishing pneumoperitoneum during laparoscopic abdominal surgery," *Cochrane Database Syst. Rev.*, no. 3, Art. no. CD009569, 2022.
[58] K. Draper *et al*., "Duration of postlaparoscopic pneumoperitoneum," *Surg. Endosc.*, vol. 11, pp. 809–811, Aug. 1997.
[59] D. S. Early *et al*., "Appropriate use of GI endoscopy," *Gastrointest. Endosc.*, vol. 75, no. 6, pp. 1127–1131, Jun. 2012.
[60] Y. Ushimaru *et al*., "The endoluminal pressures during flexible gastrointestinal endoscopy," *Sci. Rep.*, vol. 10, no. 1, Art. no. 18169, Oct. 2020.
[61] R. Wardhan *et al*., "Gas pressure from the endoscope: An unexplored contributor to morbidity and mortality?," *Cureus*, vol. 14, no. 11, Art. no. e31779, Nov. 2022.
[62] D. Popa *et al*., "Iatrogenic arterial gas embolism from esophagogastroduodenoscopy," *J. Emerg. Med.*, vol. 57, no. 5, pp. 683–688, Nov. 2019.
[63] S. Jayaraman *et al*., "The association between central venous pressure, pneumoperitoneum, and venous carbon dioxide embolism in laparoscopic hepatectomy," *Surg. Endosc.*, vol. 23, pp. 2369–2373, Oct. 2009.
[64] V. J. Orhurhu *et al*., "Carbon dioxide embolism," in *StatPearls* [Online]. Treasure Island, FL, USA: StatPearls Publishing, 2019. Available: https://www.ncbi.nlm.nih.gov/books/.
[65] A. Haggerty and M. Nirmalan, "Capillary dynamics, interstitial fluid and the lymphatic system," *Anaesth. Intensive Care Med.*, vol. 23, no. 2, pp. 130–137, Feb. 2022.
[66] N. Radhakrishnan, "The pathophysiology of varicose veins of the lower limb," in *Genesis, Pathophysiology and Management of Venous and Lymphatic Disorders*, N. Radhakrishnan, Ed. Amsterdam, The Netherlands: Elsevier, 2022, ch. 5, pp. 95–137.
[67] T. Merkel *et al*., "Gas sorption, diffusion, and permeation in poly(2,2-bis(trifluoromethyl)-4,5-difluoro-1,3-dioxole-co-tetrafluoroethylene)," *Macromolecules*, vol. 32, no. 25, pp. 8427–8440, Dec. 1999.
[68] D. Fuard *et al*., "Optimization of poly(dimethylsiloxane) (PDMS) substrates for studying cellular adhesion and motility," *Microelectron. Eng.*, vol. 85, nos. 5–6, pp. 1289–1293, May–Jun. 2008.
[69] R. Baudoin *et al*., "Parallelized microfluidic biochips in multi well plate applied to liver tissue engineering," *Sens. Actuators B Chem.*, vol. 173, pp. 919–926, Oct. 2012.
[70] R. Ariati *et al*., "Polydimethylsiloxane composites characterization and its applications: A review," *Polymers*, vol. 13, no. 23, Art. no. 4258, 2021.
[71] T. Tsuzuki, K. Baassiri, Z. Mahmoudi, and D. V. Nicolau, "Hydrophobic recovery of PDMS surfaces in contact with hydrophilic entities: Relevance to biomedical devices," *Materials*, vol. 15, no. 24, Art. no. 8752, 2022.

[72] F. Khan *et al*., "Artificial blood: The history and current perspectives of blood substitutes," *Discoveries*, vol. 8, no. 1, Art. no. e104, 2020.
[73] "Blood flow, blood pressure and resistance." Accessed: [insert access date]. [Online]. Available: https://pressbooks.bccampus.ca/kins1100/chapter/blood-flow-blood-pressure-and-resistance/
[74] V. R. Jacobs *et al*., "Intraoperative evaluation of laparoscopic insufflation technique for quality control in the OR," *JSLS*, vol. 4, no. 3, pp. 189–193, 2000.
[75] J. Y. Lee and S. J. Lee, "Murray's law and the bifurcation angle in the arterial micro-circulation system and their application to the design of microfluidics," *Microfluid. Nanofluid.*, vol. 8, no. 1, pp. 85–95, Jan. 2010.
[76] T. F. Sherman, "On connecting large vessels to small," *J. Gen. Physiol.*, vol. 78, no. 4, pp. 431–453, Oct. 1981.
[77] S. Lorthois, F. Lauwers, and F. Cassot, "Tortuosity and other vessel attributes for arterioles and venules of the human cerebral cortex," *Microvasc. Res.*, vol. 91, pp. 99–109, Jan. 2014.
[78] K. Baassiri, and D. V. Nicolau, "Understanding the Impact of Synthetic Hematocrit Levels and Biomimetic Channel Widths on Bubble Parameters in Vascular Systems on a Chip," vol. 10, no. 2, p. 98, 2025.
[79] D.N. Espinoza, J.C. Santamarina, "Water-CO_2-mineral systems: Interfacial tension, contact angle, and diffusion – Implications to CO_2 geological storage," *Water Resour. Res.*, vol. 46, no. 7, July 2010.
[80] E. Hrncir, J. Rosina, "Surface tension of blood," *Physiol. Res.*, vol. 46, pp. 319-321, 1997.
[81] M.M. Mardanpour *et al.*, "Investigation of air bubble behaviour after gas embolism events induced in a microfluidic network mimicking microvasculature," *Lab Chip*, vol. 24, no.9, pp. 2518-2536, April 2024.
[82] X. He *et al.*, "Non-condensable gas bubble dissolution with a modified tunable surface tension multicomponent lattice Boltzmann model," *Comput. Fluids*, vol. 233, January 2022.
[83] B. Olaiya and D. G. Adler, "Air embolism secondary to endoscopy in hospitalized patients: results from the National Inpatient Sample (1998-2013)," *Ann. Gastroenterol.,* vol. 32, no. 5, p. 476, 2019.
[84] M. A. Mirski *et al*., "Diagnosis and treatment of vascular air embolism," *Anesthesiology*, vol. 106, no. 1, pp. 164–177, Jan. 2007.
[85] A. A. Kader and M. E. Saltveit, "Respiration and gas exchange," in *Postharvest Physiology and Pathology of Vegetables*, 2nd ed., J. A. Bartz and J. K. Brecht, Eds. New York, NY, USA: Marcel Dekker, 2002, pp. 31–56.
[86] K. Mayer *et al*., "Cardiopulmonary responses to experimental venous carbon dioxide embolism," *Surg. Endosc.*, vol. 12, no. 8, pp. 1025–1030, Aug. 1998.
[87] P. Shah and M. A. Louis, "Physiology, central venous pressure," in *StatPearls* [Online]. Treasure Island, FL, USA: StatPearls Publishing, 2024. Available: https://www.ncbi.nlm.nih.gov/books/
[88] R. Chaudhry *et al*., "Physiology, cardiovascular," in *StatPearls* [Online]. Treasure Island, FL, USA: StatPearls Publishing, 2022. Available: https://www.ncbi.nlm.nih.gov/books/
[89] W. Maue-Dickson, "Section II. Anatomy and physiology," *Cleft Palate J.*, vol. 14, no. 4, pp. 270–287, Oct. 1977.
[90] R. Maselli *et al*., "Microvasculature of the esophagus and gastroesophageal junction: Lesson learned from submucosal endoscopy," *World J. Gastrointest. Endosc.*, vol. 8, no. 19, pp. 690–696, Nov. 2016.
[91] G. T. Reijnders-Boerboom *et al*., "Low intra-abdominal pressure in laparoscopic surgery: A systematic review and meta-analysis," *Int. J. Surg.*, vol. 109, no. 5, pp. 1400–1411, 2023.
[92]https://www.eubs.org/documents/DHM%20Sep2012%20Suppl%20Treatment%20tables.pdf
[93] M. Sawdon and E. Kirkman, "Capillary dynamics and the interstitial fluid–lymphatic system," *Anaesth. Intensive Care Med.*, vol. 18, no. 6, pp. 309–315, Jun. 2017.
[94] H. Minasyan, "Bactericidal capacity of erythrocytes in human cardiovascular system," *Int. Clin. Pathol. J.*, vol. 2, Art. no. 00052, 2016.
[95] G. T. Feke *et al*., "Blood flow in the normal human retina," *Invest. Ophthalmol. Vis. Sci.*, vol. 30, no. 1, pp. 58–65, Jan. 1989.
[96] R. N. Palchesko *et al*., "Development of polydimethylsiloxane substrates with tunable elastic modulus to study cell mechanobiology in muscle and nerve," *PLoS One*, vol. 7, no. 12, Art. no. e51499, Dec. 2012.
[97] R. T. Yen and S. S. Sobin, "Elasticity of arterioles and venules in postmortem human lungs," *J. Appl. Physiol.*, vol. 64, no. 2, pp. 611–619, Feb. 1988.
[98] L. Xu *et al*., "Vacuum-driven power-free microfluidics utilizing the gas solubility or permeability of polydimethylsiloxane (PDMS)," *Lab Chip*, vol. 15, no. 20, pp. 3962–3979, Oct. 2015.
[99] S. Kanehashi *et al*., "Microstructure and gas diffusivity of poly(dimethylsiloxane) dense membrane using molecular dynamics simulation," *Trans. Mater. Res. Soc. Jpn.*, vol. 37, no. 3, pp. 439–442, 2012.
[100] A. S. Popel, "Theory of oxygen transport to tissue," *Crit. Rev. Biomed. Eng.*, vol. 17, no. 3, pp. 257–321, 1989.
[101] A. Vadapalli, R. N. Pittman, and A. S. Popel, "Estimating oxygen transport resistance of the microvascular wall," *Am. J. Physiol. Heart Circ. Physiol.*, vol. 279, no. 2, pp. H657–H671, Aug. 2000.
[102] D. A. Markov *et al*., "Variation in diffusion of gases through PDMS due to plasma surface treatment and storage conditions," *Biomed. Microdevices*, vol. 16, no. 1, pp. 91–96, Feb. 2014.
[103] S. O. Woo *et al*., "Molecular diffusion analysis of dynamic blood flow and plasma separation driven by self-powered microfluidic devices," *Biomicrofluidics*, vol. 15, no. 3, Art. no. 034106, 2021.
[104] C. F. Wenceslau *et al*., "Guidelines for the measurement of vascular function and structure in isolated arteries and veins," *Am. J. Physiol. Heart Circ. Physiol.*, vol. 321, no. 1, pp. H77–H111, Jul. 2021.
[105] J. R. Levick, "Overview of the cardiovascular system," in *An Introduction to Cardiovascular Physiology*. Oxford, U.K.: Butterworth-Heinemann, 1991, ch. 1, pp. 1–1.

This article has been accepted for publication in IEEE Transactions on Biomedical Engineering. This is the author's version which has not been fully edited and content may change prior to final publication. Citation information: DOI 10.1109/TBME.2026.3729588